Selective Adsorption of Functionalized Nanoparticles to Patterned Polymer Brush Surfaces and Its Probing with an Optical Trap

Annina Steinbach,[a] Tobias Paust,[b] Manuela Pluntke,[b] Othmar Marti,[b] and Dirk Volkmer*[a]

The site-specific attachment of nanoparticles is of interest for biomaterials or biosensor applications. Polymer brushes can be used to regulate this adsorption, so the conditions for selective adsorption of phosphonate-functionalized nanoparticles onto micropatterned polymer brushes with different functional groups are optimized. By choosing the strong polyelectrolytes poly(3-sulfopropyl methacrylate), poly(sulfobetaine methacrylate), and poly[2-(methacryloyloxy)ethyl trimethylammonium chloride], it is possible to direct the adsorption of nanoparticles to specific regions of the patterned substrates. A pH-dependent adsorption can be achieved by using the polycarboxylate brush poly(methacrylic acid) (PMAA) as substrate coating. On PMAA brushes, the nanoparticles switch from attachment to the brush regions to attachment to the grooves of a patterned substrate on changing the pH from 3 to 7. In this manner, patterned substrates are realized that assemble nanoparticles in pattern grooves, in polymer brush areas, or substrates that resist the deposition of the nanoparticles. The nanoparticle deposition can be directed in a pH-dependent manner on a weak polyelectrolyte, or is solely charge-dependent on strong polyelectrolytes. These results are correlated with surface potential measurements and show that an optical trap is a versatile method to directly probe interactions between nanoparticles and polymer brushes. A model for these interactions is proposed based on the optical trap measurements.

1. Introduction

Polymeric nanoparticles came into the focus of materials science as drug-carrier systems in the 1980s.[1] They can lower the necessary amount of the applied drug or even make pharmaceuticals with inappropriate properties available by masking their adverse pharmacokinetics.[2] However, applications of nanoparticles are not restricted to pharmacological products but may also include nano- and micro-scale technological systems. For example, biosensors and medical diagnostic devices will probably benefit from the controlled adhesion and adsorption of labeled or catalytic nanoparticles into ordered arrays.[3] Thus, our approach in tailoring the interactions between polymeric nanoparticles and chemically designed surfaces holds promise for the next generation of sensors and diagnostic devices.

Polymer brushes are surface-tethered polymer chains forming an extremely thin polymer film, which can, nevertheless, significantly alter surface properties. By synthesizing the polymer brushes through surface-initiated atom-transfer radical polymerization (SI-ATRP), it is simple to introduce a plethora of functional groups, charged as well as non-charged, and polar as well as nonpolar groups.[4,5] Until now, only a few studies have been concerned with the assembly of polymeric nanoparticles on polymer-modified substrates. Most research groups have focused their investigations on the incorporation of inorganic nanoparticle materials into a polymer matrix.[6–9] The interaction of polymeric nanoparticles with polymer coatings has been addressed in only a few studies that dealt with layer-by-layer-deposited polyelectrolyte films. In these studies, the surface-directed adsorption of nanoparticles displayed a strong dependence on pH, ionic strength, and surfactants.[10,11] These studies, however, do not report a more detailed description of the forces acting between the nanoparticles and the polymer surfaces. In the present work, an optical trap setup was used to provide the means for examining the nanoparticle surface interactions in a more quantitative way.

Particles were first trapped in a strongly focused laser beam in the 1980s.[12] Since then, optical trapping has found many applications in molecular biology, biophysics, and medicine, ranging from active microrheology in biopolymer networks[13] to manipulation of biological molecules[14] and DNA.[15,16] Information about the mechanical properties of these systems can be gathered by the use of small tracer particles.[17,18] With an optical trap and a trapped particle, it is possible to apply forces in the picoNewton range to the observed object. The displacement of the trapped particle from its equilibrium position can then be detected with a positioning precision in the nanometer range with a high bandwidth.[19] Therefore, use of

[a] A. Steinbach, Prof. Dr. D. Volkmer
Chair of Solid State and Materials Chemistry
Institute of Physics, University of Augsburg
Universitätsstr. 1, 86159 Augsburg (Germany)
E-mail: dirk.volkmer@physik.uni-augsburg.de

[b] Dr. T. Paust, Dr. M. Pluntke, Prof. Dr. O. Marti
Institute of Experimental Physics
University of Ulm, Albert-Einstein-Allee 11
89081 Ulm (Germany)

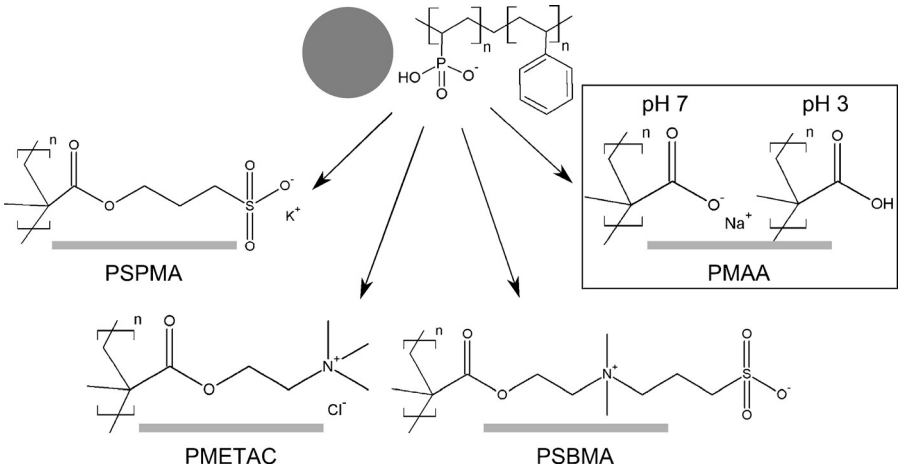

Figure 1. Schematic overview of the polymers used to assemble phosphonate-functionalized nanoparticles. The phosphonate nanoparticles were adsorbed onto patterned polysulfonate (PSPMA), polyamine (PMETAC), polysulfobetaine (PSBMA), and polycarboxylate (PMAA) brushes (see text for details). The latter showed a pH-dependent adsorption behavior on varying the solution pH value from 3 to 7.

a well-established optical-trap setup is a feasible solution to directly measure the interactions between nanoparticles and polymer brushes or other surfaces.

Herein, an approach is presented towards the selective deposition of phosphonate-functionalized polystyrene (PS) nanoparticles, with a 150 nm diameter, onto flat surfaces modified with micropatterned polymer brushes containing pattern widths ranging from 2.5 to 160 μm (Figure 1). Strong-electrolyte polymer brushes with quaternary amine, sulfobetaine, and sulfonate groups as well as weak polyelectrolytes with carboxylate groups were used to study the influence of charge and pH on the interactions between the polymer brushes and the phosphonate-functionalized nanoparticles. To realize a more quantitative description of the interactions between the nanoparticles on surface-grafted polymer brushes, they were measured with an optical trap. With this approach, the application range of this method is augmented and a useful tool for the development of composite polymer coatings for future bio- and nanomaterials is presented.

2. Results and Discussion

To find a feasible procedure for the selective deposition of phosphonate-functionalized nanoparticles as a monolayer onto flat surfaces covered with microstructured polymer brushes, three key parameters were optimized: the solids content of the colloid, that is, its phosphonate nanoparticle content; the pH during nanoparticle attachment and the washing steps; and finally the functional groups of the polymer brushes. The nanoparticles comprised the fluorescent dye *N*-(2,6-diisopropylphenyl)perylene-3,4-dicarbonacidimide (PMI), which provided the means to use fluorescence microscopy as a fast method to determine the distribution of the nanoparticles on the patterned substrates. Scanning electron microscopy (SEM) offered a closer look at the selective adsorption of these nanoparticles.

The first parameter, the ideal colloidal solid content during immersion of the polymer brush substrates, was determined to be 1 mg mL^{-1}. This amount of phosphonate nanoparticles in the colloid yielded a monolayer with a uniform distribution. Higher solids contents produced multilayers, whereas lower solids contents increased irregularities and uneven distributions.

Charge-Directed Deposition of Phosphonated Nanoparticles onto Microstructured Polymer Brush Surfaces

To direct the phosphonate nanoparticle adsorption independently of the pH of the colloidal suspension, the strong polyelectrolytes poly(3-sulfopropyl methacrylate) (PSPMA), poly(sulfobetaine methacrylate) (PSBMA), and poly[2-(methacryloyloxy)ethyl trimethylammonium chloride] (PMETAC) were used to build up thin films of polymer brushes. The functional groups of these polymers, namely sulfonate groups and quaternary amines, were permanently charged over the whole pH range studied. The adsorption was carried out at pH 3 and the washing procedure at pH 3 and 7. For the pH values tested, there was no perceivable difference in nanoparticle distribution for these strong polyelectrolyte brushes.

Attachment of phosphonate nanoparticles to areas covered by the negatively charged PSPMA brushes was not observed, but bright spots of unspecific aggregated nanoparticles was seen (Figure 2 A). Therefore, it can be concluded that the negative charges on the phosphonate nanoparticles as well as on the sulfonate substrate prevented any attractive interactions. Between the two negatively charged surfaces, repelling forces did not allow for adsorption.

The polycationic PMETAC electrolyte directed the nanoparticles towards the areas covered with the polymer brush (Figure 2 B). As positive charge attracts negative charge, the PMETAC brushes carrying positively charged quaternary ammonium groups directed the phosphonate nanoparticles to these regions. Owing to the permanent charge, this ionic binding was independent of the pH.

In contrast, on zwitterionic PSBMA substrates, the nanoparticle adsorption occurred preferentially in the grooves (Figure 2 C). Zwitterionic PSBMA brushes have both negatively and positively charged groups. Thus, no electrostatic interaction prevailed that could interact with the charged and hydrophilic nanoparticles. The charged groups of the polymer brushes were also hydrated in the swollen state, thus hampering direct interactions between the charged groups of the brush and the nanoparticles.[20,21] The competing surface in the groove areas contained irradiated surface-bound initiator. The irradiated ini-

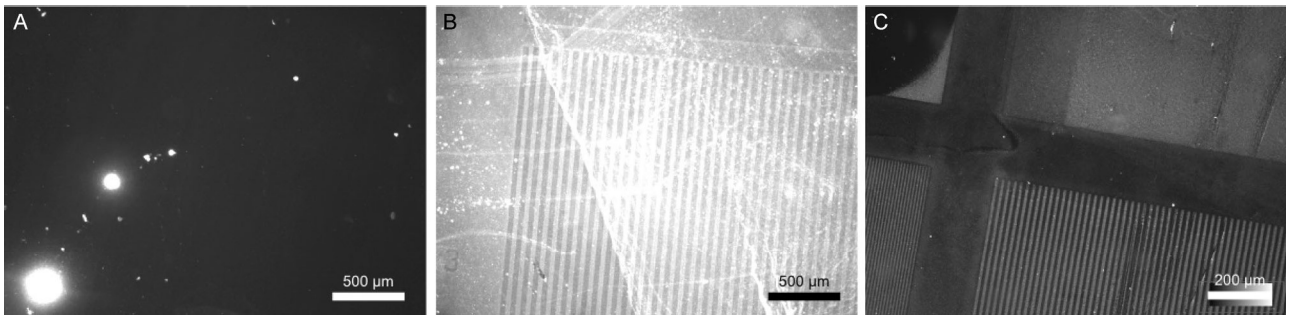

Figure 2. Fluorescence micrographs with high fluorescence indicated by bright spots. A) Microstructured PSPMA sample after immersion in the colloid and washing; only unspecific aggregates of nanoparticles are visible; scale bar 500 µm. B) Nanoparticles on a microstructured PMETAC sample showing preferred attachment to polymer brush regions; scale bar 500 µm. C) Nanoparticle adsorption on a PSBMA substrate with a strong preference for directing phosphonate nanoparticle adsorption to the grooves; scale bar 200 µm.

tiator is hydrophilic (water contact angle 27°; see also the Supporting Information Figures S1 and S2, Table S1, and Note S1), but it is not able to swell, and therefore, it is able to interact with the phosphonate nanoparticles.

Additionally, if the PSBMA brushes swell in good solvents, such as water and phosphate-buffered saline (PBS), they can reach a thickness in the range of the phosphonate nanoparticles' diameter (up to 120 nm in water).[22–24] The nanoparticles could, therefore, be entrapped in the grooves by the swollen PSBMA brush walls surrounding the 2.5 to 160 µm-wide grooves.

Both effects—the better possible interactions between the phosphonate nanoparticles and the groove surface as well as the mechanical entrapping by polymer brush walls—may be the reason for the observation that nanoparticle attachment occurred preferentially in the grooves.

pH-Dependent Adsorption of Phosphonate Nanoparticles

Next to the systems that directed the adsorption of phosphonate nanoparticles irrespective of the pH, the adsorption behavior to surfaces consisting of the weak polyelectrolyte poly(methacrylic acid) (PMAA), carrying carboxylate groups, was investigated. The nanoparticle attachment process comprised two steps: the immersion of the PMAA substrate in the colloidal suspension containing the phosphonate nanoparticles, and a washing step to remove any excess colloids. The adsorption step, that is, immersion in the colloid, always took place at pH 3, whereas the washing steps were carried out at either pH 7.4 in PBS or at pH 3.0 in dilute aqueous hydrochloric acid (HCl). Keeping the sample at pH 3 for the washing step after adsorption led to attachment of the nanoparticles almost exclusively to the polymer brush regions (Figure 3A and B). In contrast, on changing the pH to a value of 7.4 for the washing step, the attachment of the nanoparticles was restricted to the grooves (Figure 3C and D). Thus, the phosphonate nanoparticles showed a selective attachment to micropatterned PMAA brushes, which was dependent upon the pH value of the washing solvent.

To explain this behavior, the surface potentials of the interacting materials were measured. The zeta potential of the

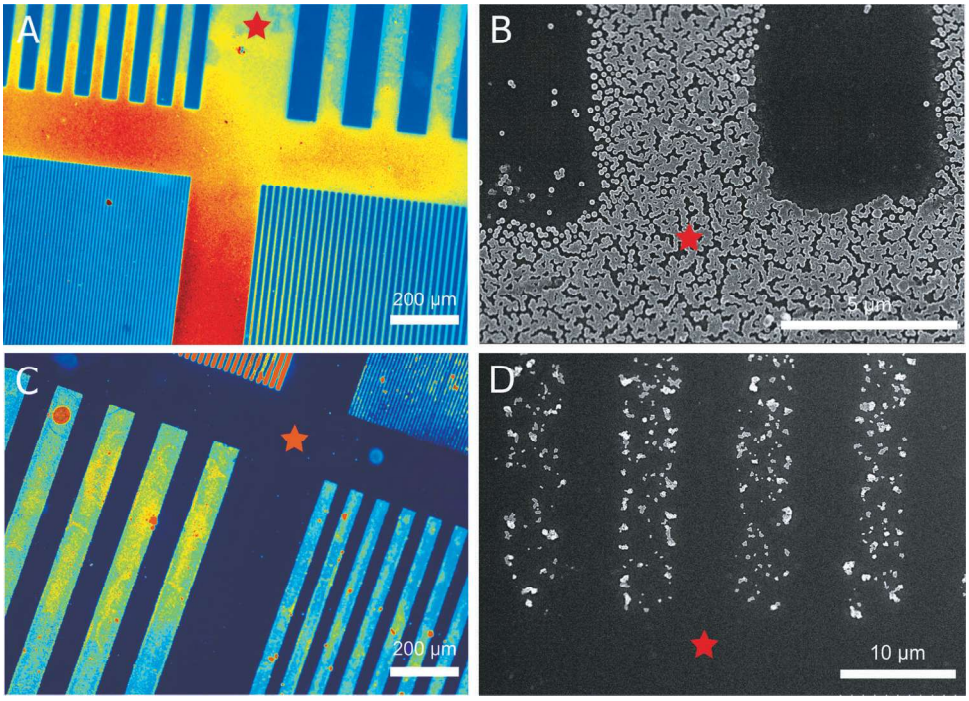

Figure 3. Selective adsorption of phosphonate nanoparticles loaded with a fluorescent dye on PMAA brushes with a linear stripe pattern. The surface areas covered by the PMAA brush are marked with a red star. A) Pseudocolor fluorescence micrograph of the nanoparticle distribution after adsorption and washing steps at pH 3: adsorption to polymer brush regions; red color indicates a high fluorescence intensity, blue a low intensity; scale bar 200 µm. B) Corresponding SEM image; scale bar 5 µm. C) Fluorescence micrograph of a sample washed at pH 7: adsorption to the grooves; scale bar 200 µm. D) Corresponding SEM image; scale bar 10 µm.

phosphonate-functionalized nanoparticles varied only slightly in the pH region used, that is, from −15.6 mV at pH 3 to −20 mV at pH 10.[25] This means that the PMAA brush surface properties should be the main cause for the switching behavior. The zeta potential of the polymer brush dropped from nearly 0 mV at pH 3 to around −30 mV at pH 7, as confirmed by streaming potential measurements. Therefore, the PMAA brush surface area was not charged at pH 3. At pH 7, however, the surface potential was highly negative and the PMAA chains were predominantly deprotonated.

On the basis of these results, it can be hypothesized that the protonation and deprotonation of the relevant carboxylic acid was the driving force for the observed interaction pattern. At pH 3, the major part of the carboxylate groups of the PMAA brush is protonated and acts as a non-charged hydrogen-bond donor. The phosphonic acid groups on the nanoparticles are partly deprotonated at pH 3 ($pK_{a1}=1.8$, $pK_{a2}=7.3$) and can equally contribute to hydrogen bonding. Thus, strong interactions between the phosphonate and the carboxylic acid groups, owing to the formation of hydrogen bonds, will lead to binding of the nanoparticles to the brush (Figure 4, left). The opposite applies for pH 7, at which both types of functional groups are negatively charged. Owing to the electrostatic repulsion, no attachment to the polymer brush regions is possible (Figure 4, right).

At this point, the question remains why the phosphonate nanoparticles could be found in the grooves and why they were not simply repelled, as was the case for the constantly negatively charged PSPMA samples (Figure 2 A). To explain this difference, it is important to remember that the immersion in the colloidal nanoparticle suspension always took place at pH 3. This first step ensures the first attraction and binding between the nanoparticles and the sample surface through hydrogen bonds. Otherwise, upon immersion of the substrate in a nanoparticle suspension at a higher pH value, the repulsive forces would prevail because of the negative charges, and no binding would occur between the substrate and the particles in the first place. This case is the analogue of the above-mentioned repulsion between PSPMA brushes and the nanoparticles.

Thus, it was necessary to immerse the substrates in the colloid at pH 3 to adsorb the nanoparticles to the surface. The rearrangement probably did not happen until the washing step at pH 7, and only then resulted in the observed adsorption of the phosphonate nanoparticles to the grooves. Note the lower density of the particle layer in Figure 3 D compared to the nearly close-packing observed in Figure 3 B. The reduced number of nanoparticles is, therefore, attributed to the repulsive electrostatic forces acting between the deprotonated carboxyl groups and phosphonate groups on changing the pH from a value of 3 to 7. Some of the nanoparticles probably diffused into the washing solvent. The rest of the primarily bound nanoparticles most likely rearranged on the surface and moved into the grooves (see Note S2 in the Supporting Information).

To explore a method for a more quantitative description of this switching behavior and the interactions between the nanoparticles and the PMAA brush, an optical trap setup was used. With the help of this method, it was possible to compare the PMAA brush areas with the groove areas in terms of forces acting between negatively charged nanoparticles and the respective surface. Owing to the relatively low optical contrast of the negatively charged 150 nm phosphonate particles in the light microscope, we chose to use commercially available, larger particles with a comparable negative surface potential (Figure S3 in the Supporting Information). As outlined above, the surface charge of the nanoparticles did not contribute greatly to the switching effect, so the forces observed in the optical trap should not differ considerably from the experiments described above.

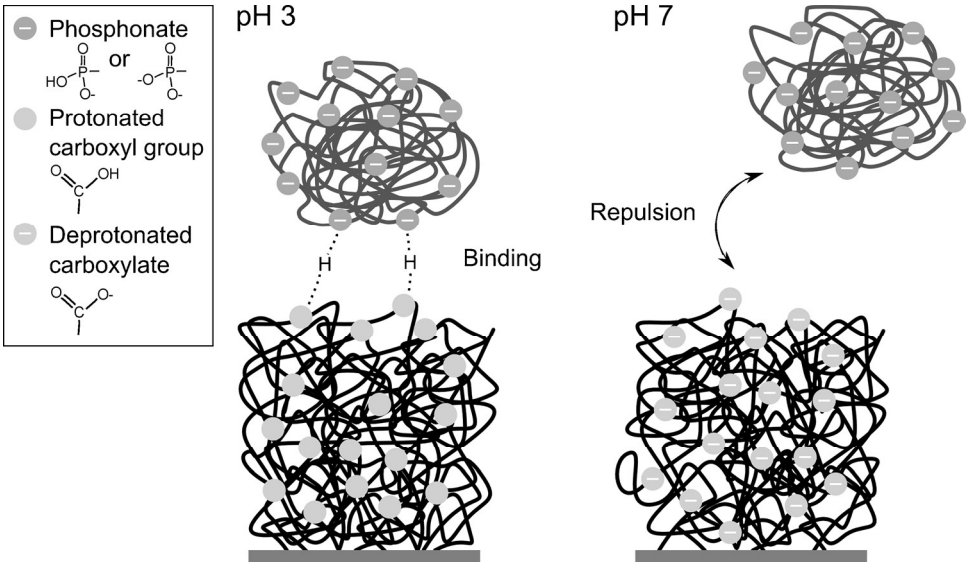

Figure 4. Sketch of the proposed model of phosphonate nanoparticles binding to micropatterned PMAA brush surfaces at pH 3 (left) and pH 7 (right). At pH 3, hydrogen bonds between the carboxylic acid groups of the brush and the partially deprotonated phosphonic acid groups of the nanoparticles cause a strong preference of the nanoparticles for the brush regions; at pH 7, the charge repulsion between the phosphonate nanoparticles and the carboxylate brush prevent deposition on the brush area.

For each measurement, a negatively charged nanoparticle was caught in the focus of the laser beam. Guided by the focus, the nanoparticle approached the surface. During this approach, the nanoparticle's displacement out of the laser focus was measured as a function of the distance between the laser focus and the surface (Figure 5).

Figure 6 A and B shows typical results from these measurements, juxtaposing approaches at pH 3 (Figure 6 A) and pH 7 (Figure 6 B). The two graphs

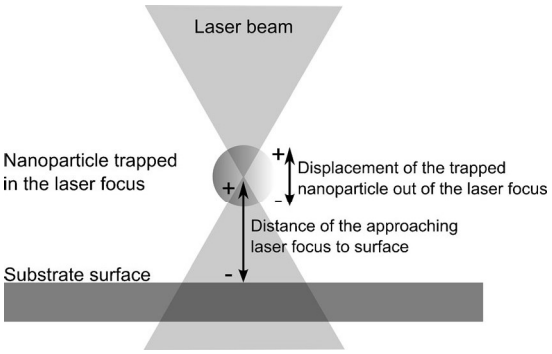

Figure 5. Schematic drawing of the laser trap with the relevant measurement parameters: the displacement of the nanoparticle out of the laser beam focus is measured at several points during the approach of the focus to the surface.

compare approaches of a negatively charged nanoparticle to the groove surface (red) with approaches to the PMAA brush surface (blue). In these graphs, the displacement of the nanoparticle out of the laser beam focus is plotted against the approach of the focus to the surface. Between the measuring points, the focus approached the surface in 5 nm steps. The insets show a zoom into the snap-in region, in which the particle is pulled towards the surface due to attractive forces. For an easier comparison of the strength of the snap-in, the displacement minima were shifted towards each other in Figure 6 A.

On comparing Figure 6 A and Figure 6 B, the change of the pH value visibly influenced the displacement of the trapped nanoparticle, which reflects the attractive forces acting on it. In Figure 6 A (measured at pH 3), the curves show a point at

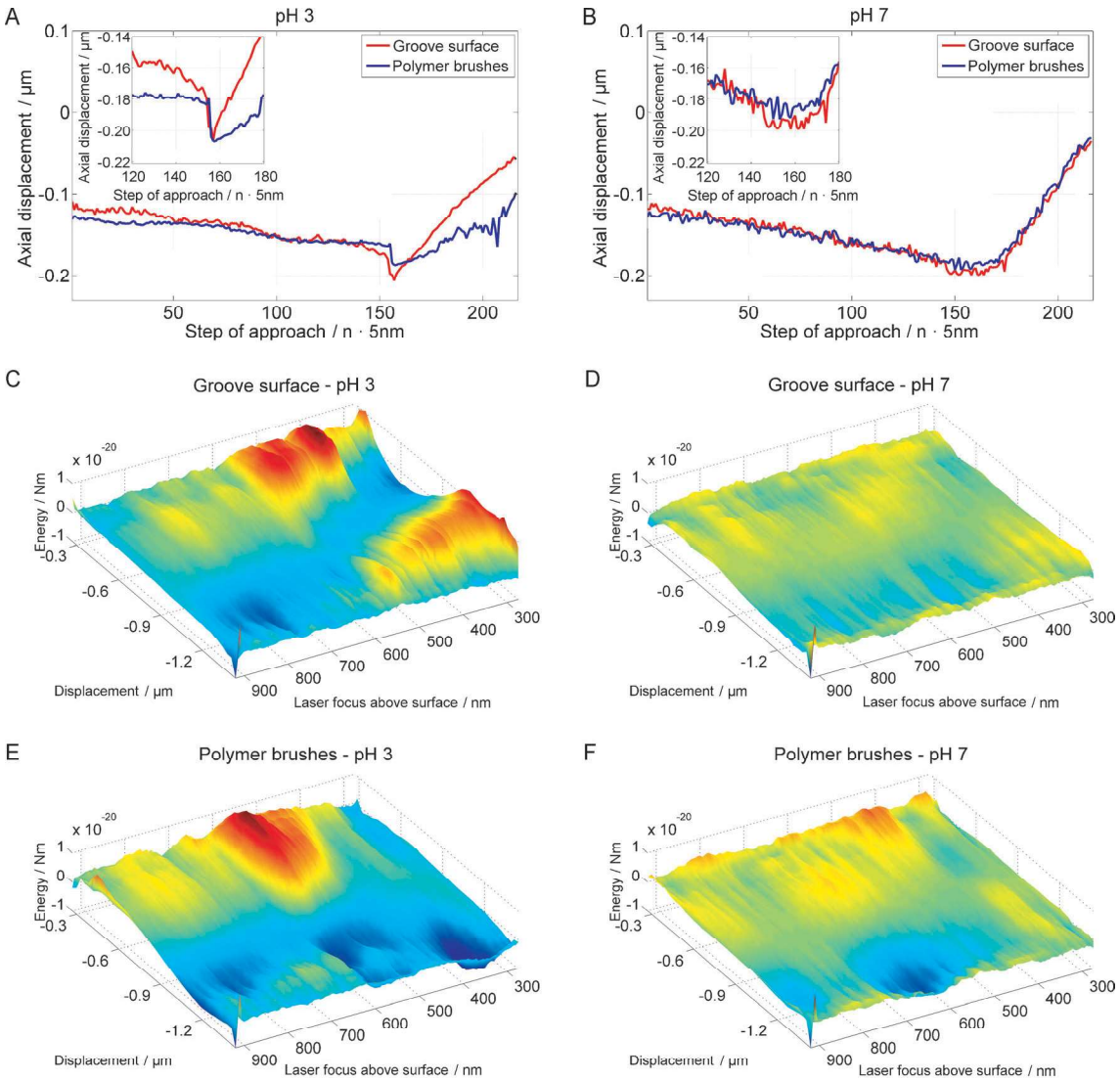

Figure 6. Response of the particles upon approaching a PMAA-coated polymer brush substrate and a groove surface at pH 3 (left) and pH 7 (right). A, B) Displacement of the particles during the approach towards the surface due to the interaction between polymer brushes (blue) and groove surface (red). The insets depict a close-up of the snap-in for all cases. C–F) For every step during the approach a potential is calculated. The surfaces shown are the series of potentials that were subtracted by the optical tweezers potential. Hence, the surface depicts the influence of the brushes or the groove dependent on the axial position of the optical tweezers. The higher the potential (yellow to red), the lower is the probability of a displacement of the particles onto this region. Conversely, the lower the potential (green to blue), the more often the particles are located in that potential well.

which the particle displacement changes and reaches a minimum. This point is the above-mentioned snap-in. The measurements reveal that the polymer brush regions, as well as the groove areas, attract the nanoparticles. After the snap-in, the two substrate areas can be readily discriminated: in the grooves (red), the measurements showed a steep rise of displacement after the snap-in. The grooves are only covered by an extremely thin (about 1 nm)[22] layer of irradiated initiator. Thus, the rigid glass supporting material, determines the curve shape, with the trapped particle being pressed against the surface and staying at the surface as the laser beam focus moves further downwards. The blue line shows, by the more slowly increasing displacement, how the particle dips into the soft PMAA brush film.

The curve in Figure 6B was obtained at pH 7 and shows no snap-in and a less sharp minimum, thus indicating that less attractive forces acted in this case. Here, the trapped nanoparticle gets slowly and evenly displaced out of the trap until attaining the minimum at which the surface is reached. Further approaching the surface after the snap-in, the nanoparticle was pushed against the surface by the optical trap. In contrast to our expectations, the two approaches, to the brush and the groove surface, did not differ at pH 7.

However, a difference between the glass surface and the polymer field can be observed if the potentials are calculated from the measured data and plotted against the displacement and the approach. The potentials shown in Figure 6C–F depict the net potential with the trap potential subtracted from the total potential measured. This net potential reflects the influence of only the groove surface or the polymer brush on the axial motion of the approaching particle.

Figure 6C shows the axial net potential during the approach to the groove surface at pH 3. The steep potential walls, especially at larger displacements, show that a force constrains the nanoparticle motion. After the snap-in, when the trap pushes the nanoparticle against the surface, the potential moves towards larger values of nanoparticle displacement in the positive *z* direction (see Figure 5).

In Figure 6E, the same behavior can be observed on movement of the particle towards an area covered with PMAA brush, but after the snap-in the potential landscape differs from the one on groove surfaces (Figure 6C). The potential minimum does not move to large displacement values but to lower ones, that is, nearer to the substrate surface. At the same time, the potential walls get less steep, showing that the particle can move inside the field and reflecting the mobility and lower stiffness of the polymer brush.

Comparison of the PMAA brush surface to the groove surface at pH 3 shows that both surfaces attract the negatively charged nanoparticles. However, the potential well of the brush region is close to the surface over the whole measurement range, whereas in the groove regions the potential well moves away from the surface upon approaching it more closely. The number of nanoparticles will be greatest in the potential minima. Over the PMAA brush surface the potential well is close to the surface over the whole approach distance, which means that the nanoparticles are drawn to the surface over this distance. Over the groove surface, however, this strong attraction is missing. Therefore, the optical-trap measurements reflect the nanoparticles' preference for the brush regions over the grooves at pH 3.

If the particle approaches the two surfaces at a pH value of 7 (Figure 6D and F), the potentials show a similar behavior. However, the spatial constraints are lower because the attractive forces are smaller. Also, the potential wall of the surface is steeper for the polymer brush than for the groove surface. At the same time, in both measurements, the potential minima are located after the snap-in. This contradicts the distinct distribution pattern that the system shows at pH 7 (Figure 3D), in which the nanoparticles are only found in the grooves and not on the PMAA brush areas.

The energy minima of the groove surface and the polymer brush field progress quite similarly upon approach. The progress of the minima also resembles the potential landscape of the approach to the groove at pH 3 in Figure 6C. Both potential landscapes at pH 7 lack the pronounced potential well, pulling the nanoparticle towards the surface after the snap-in (see Figure 6E). This lack of firm interaction indicates that the nanoparticles did not adhere strongly to both the brush areas and the grooves, and were thus prone to desorption and rearrangement. At the same time, the brush surface has a more pronounced potential well for displacement away from the surface upon nearer approach. However, this does not explain why the nanoparticles can be found in the grooves (Figure 3D).

Although no distinct attractive forces can be measured with the optical trap, the location of the nanoparticles in the grooves can still be explained. If the location of nanoparticles in the grooves was not caused by measurable forces, it might be a mechanical factor that holds the nanoparticles in the grooves. The interactions between the nanoparticles and the PMAA brush at pH 7 could be analogous to the interactions between the nanoparticles and the zwitterionic PSBMA brush. It is known that the PMAA brush used here extends to about 300 nm in height when in equilibrium after 1 h in PBS. It extends to even greater heights (up to 1000 nm) before equilibrium is reached.[22] The equilibrium height of the PMAA brush in PBS is, therefore, twice the diameter of the nanoparticles, and poses a considerable barrier to the nanoparticles. The pattern might simply prevent the nanoparticles from being washed off, and thus, retain some of them in the 2.5 to 160 μm-wide grooves surrounded by the high polymer brush walls.

In summary, the interactions between the PMAA brush and phosphonate nanoparticles can be pictured as follows: at pH 3, the phosphonate nanoparticles are adsorbed to the polymer brush. Then, the pH is changed to a value of 7 for the washing step, which disrupts the bonding between the surface and the nanoparticles. In the resulting labile situation, most particles are washed off, except those that are held on the substrate by the polymer brush walls around the groove.

On evaluating the method, there was a small constraint in the measuring system, because it was not possible to use the original nanoparticles for the laser-trap measurements. Further improvements, such as a better matching of the nanoparticle

labeling and the laser trap microscope, and optimization can probably eliminate this drawback. Moreover, effects based on mechanical parameters, rather than on specific forces, could not be measured with the optical trap. Another point that can pose difficulties is the finding of the optimal parameter range of the optical trap to measure small forces. The higher the trapping force, the lower is the sensitivity for the interacting forces between surface and nanoparticle by which the particle gets displaced. In the case of a weak trapping force, smaller interacting forces can be measured, but the Brownian motion of the particle becomes stronger and disturbs the measurement. An optimum can be found by performing several test measurements and by varying the trapping force.

Despite small flaws, the method is proven to be a practical tool to observe forces that contribute to self-assembly processes and should serve well for the development of new nanomaterials. The optical tweezers represent a useful tool to measure the potential of a particle and its displacement and are, therefore, suitable to determine the forces acting between a particle and a surface. The high precision, which is achieved in determining the motion of the particle, leads to a high accuracy in the measurement of interaction forces that are in the range of picoNewtons down to several hundreds of femtoNewtons.

3. Conclusions

The reported experiments show that polymer brushes can be a versatile tool to modify and pattern a surface, and to subsequently selectively deposit polymeric phosphonate nanoparticles. Permanently charged polymers, such as PMETAC, PSBMA, and PSPMA, can direct nanoparticle adsorption, independent of the pH value. The adsorption can be controlled by the pH value upon using PMAA brushes. In this case, nanoparticles are attracted to the surface at pH 3 and deposited on the brush upon washing at pH 3, or in the grooves of the patterned coating if washing steps are carried out at pH 7. This is explained by the protonation state of the polymer brush, which has its isoelectric point at around pH 3 and is thus protonated, whereas it is completely deprotonated at pH 7. Biosensors might be a promising field of application for these composite surfaces, strictly confining reagents to certain areas on the micrometer scale. Moreover, the application range of the optical trap method is extended to measure the small forces of interacting surfaces, which can have an impact on the buildup of new nanomaterials by elucidating the mechanisms of self-assembling systems.

Experimental Section

Materials

2-(Methacryloyloxy)ethyl trimethylammonium chloride (METAC) was purchased from Aldrich and treated with aluminum oxide prior to use. PBS, *N*,*N*-dimethylformamide p.a., potassium 3-sulfopropyl methacrylate (SPMA), sodium methacrylate (NaMAA), 2,2′-bipyridine p.a., CuBr, and CuCl were obtained from Aldrich and used as received. Microscope glass slides (Menzel), *N*-(3-sulfopropyl)-*N*-methacroyloxyethyl-*N*,*N*-dimethylammonium betaine (SBMA), methanol p.a., $CuBr_2$, and $CuCl_2$ were acquired from Merck/VWR and used as received. Water was obtained by using a TKA Smart2-Pure Millipore machine.

Synthesis of Microstructured Polymer Brush Substrates

For the preparation of microstructured polymer brush substrates, cleansed microscope glass slides were coated with a self-assembled monolayer (SAM) of an atom-transfer radical polymerization (ATRP) initiator. The microstructure was obtained by inactivating the initiator in designated regions by irradiation with UV light through a custom-made chrome-coated quartz mask. The nonirradiated areas served as starting points for the SI-ATRP of NaMAA, which resulted in polycarboxylate brushes. The procedure was described in detail by Tugulu et al.[26] Accordingly, samples with the irradiated initiator SAM served as substrates for the SI-ATRP of monomers with other functional groups. These were the strong electrolyte SPMA, the sulfobetaine SBMA, and the positively charged amine METAC. To obtain PSPMA, the protocol of Masci et al.[27] was adapted to a surface-initiated reaction. SBMA was polymerized following the protocol of Azzaroni et al.[28] The guideline for the METAC polymerization was the work of Zhou et al.[29] Briefly, the respective monomer was dissolved in a dimethyl formamide/water mixture (PSPMA) or a methanol/water mixture (PSBMA and PMETAC). The solution was degassed with at least three freeze–pump–thaw cycles and a catalyst system containing bipyridine and $Cu^{+}$and Cu^{2+} ions was added. The initiator-coated glass substrates were immersed in this solution for 2 h (PSBMA) or 16 h (PSPMA and PMETAC). To quench the polymerization, the solution was exchanged with water, and the substrates were rinsed with an excess of water and washed at least three times for 2 h with water and PBS to remove any unbound polymer and remaining catalyst.

Synthesis of the Nanoparticles

Phosphonate-functionalized PS nanoparticles loaded with the fluorescent PMI dye were provided by the Landfester group, Max Planck Institute for Polymer Science, Mainz, who synthesized the nanoparticles by free-radical polymerization in a miniemulsion.[25] The main polymer of the nanoparticles was PS, which was copolymerized with 10% vinylphosphonic acid (VPA), leading to copolymer nanoparticles in which the phosphonate groups arranged at the particles' surface. The added fluorescent dye served as a label for a quick analysis of the distribution of the nanoparticles attaching to the structured substrates.

Assembly of the Nanoparticles on the Polymer Brush Substrates

A colloidal suspension of the PS-*co*-PVPA nanoparticles was diluted to a solids content of 1 mg mL^{-1}, as this was found, experimentally, to yield a monolayer with a clear adsorption pattern on the polymer brush surfaces. Higher solids contents resulted in the formation of multiple layers of nanoparticles stacked on top of each other. To adjust the pH value of the solution, HCl was added until a pH value of 3 was achieved to ameliorate adsorption on the substrate. To adsorb the nanoparticles to the patterned polymer brush coating, the substrates were immersed in the diluted nanoparticle colloid for 2 h (PMAA) or 6 h (PSPMA, PSBMA, and PMETAC) while the glass slides were mounted vertically. After immersion, the substrates were agitated briefly in either PBS (pH 7.4) or dilute HCl (pH 3.0) and washed in the same solvent, stirring constantly overnight.

Analytical Methods

Owing to the integrated PMI fluorescent dye, the distribution of the nanoparticles on the substrate was visible with a fluorescence microscope. This provided a simple and fast method to examine the adsorption pattern, and left the sample unmodified for further analysis and applications. We used an Olympus IX70 with an Abrio fluorescence system and excitation filters at 470–490 nm.

For a thorough analysis of the nanoparticle distribution on the structured coating, the samples were prepared to fit a Hitachi S-5200 high-resolution scanning electron microscope and sputtered with a 4 nm platinum layer. The samples were typically examined at an acceleration voltage of 10 eV.

The streaming potential of the PMAA brush was measured with an electrical analyzer (Anton Paar GmbH, Graz, Austria) by the Bellmann group, Leibniz Institute for Polymer Research, Dresden.[30,31] For the titration, HCl and KOH in 10 mM KCl solution were used at a flow rate of 150 mL min^{-1}.

Optical Trap

To build the stable optical trap that was used in this work, a laser with a wavelength of 1064 nm (neodymium-doped yttrium aluminum garnet laser, Coherent Compass 1064-500) and an objective with a high numerical aperture of 1.49 (CFI Apo TIRF 100XH, Nikon) were used. An acousto-optical deflector (AOD; DTSXY-400, AA-Opto-Electronic) and beam splitter divided the laser beam into two orthogonally polarized beams and made it possible to steer or oscillate the laser beams for dual/multiple-trap applications. The sample was placed onto a piezo stage (PI, PIMars, P-561.3DD, 45 × 45 × 15 μm), which ensured an accurate positioning of the sample in the nanometer range. A four quadrant photodiode (QPD) and measurement card (Keithley K-USB 3116, 125 kHz per channel) detected the laser signal and therefore the motion of the particle in the trap.

For each measurement, a PS particle of 1 μm diameter (Cat No. 4009A, Thermo Fisher Scientific, Waltham, MA, USA) was trapped 5 μm above the polymer brush surface with both the static (intensity 30 mW) and the dynamic trap (intensity 180 mW). To perform the trap calibration, the AOD excited the dynamic trap beam to triangular oscillations with a frequency of 1 Hz and an amplitude of 500 nm pp separately in the *x* and *y* directions. The particle trapped in the dynamic trap followed these oscillations. The four QPD of the static trap recorded the motion of the oscillating particle and provided the displacement as a voltage. As the amplitude was known, the conversion value of μm V^{-1} could be determined. To gather information about the trap forces, a particle was trapped in the static trap. The force calibration method may be called optical potential analysis,[19] and was one possible method to determine the trap stiffness. The thermal motion of the particle in the trap led to a Boltzmann distribution, which was used to calculate the strength of the trap.[32] Other methods that use the spatial oscillation of the particle in the trap and power spectral intensity analysis are also possible.[33] For the present work the first method was chosen as, in our opinion, a straightforward and undemanding way to calibrate the trap forces. For the static trap a force of 3 pN $μm^{-1}$ was applied at a laser intensity of 30 mW. Displacements of the particle due to external forces or Brownian motion could be resolved in the nanometer range.

For performing the approach to the surface, a particle (diameter 1 μm) was trapped above the surface (ca. 2.5 μm). The piezo stage reduced the distance between particle and surface in 5 nm steps. In each step, the QPD measured the thermal motion of the particle in the trap in the four channels of the QPD record with a frame rate of 125 kHz each for at least 2 s. The distribution of this motion led to the particle's potential for every step of the approach. At large distances to the surface, only the thermal motion and the trap forces acted on the particle, whereas the closer the particle was to the surface, the higher was the influence of the surface and the polymer brushes. By subtracting the trap potential at every step of the approach, the influence of the surface on the particle could be visualized. The average position of the particle in the measured thermal motion was used to determine the displacement of the particle. A change of the displacement during the approach in turn showed the forces acting on the particle.

Acknowledgements

This work was supported by the Landesstiftung Baden-Württemberg, Germany. We thank Anke Ziegler of the Landfester group of the Max Planck Institute for Polymer Research, Mainz, for the synthesis and provision of the nanoparticles; Bellmann and co-workers of the Leibniz-Institute for Polymer Research, Dresden, for the very helpful measurements of the polymer brush surface potential; Kohn, Kusterer, and Men of the Institute of Electron Devices and Circuits, University of Ulm, for the provision of the quartz masks, which enabled us to microstructure the substrates; Walter, Schmied, and Weih of the Institute of Electron Microscopy, University of Ulm, for the always friendly technical help with the electron microscopes; Schaller of the Chair of Solid State and Materials Chemistry, Lachner of the Chair of Experimental Physics, University of Augsburg, and Miller and Wiltschka of the Institute of Inorganic Chemistry II, University of Ulm, for their ready helping out with measurements.

Keywords: nanoparticles · optical traps · polyelectrolyte brushes · self-assembly · surface interactions

[1] V. Holzapfel, A. Musyanovych, K. Landfester, M. R. Lorenz, V. Mailänder, *Macromol. Chem. Phys.* **2005**, *206*, 2440.
[2] T. M. Allen, P. R. Cullis, *Science* **2004**, *303*, 1818.
[3] M. Klapper, S. Nenov, R. Haschick, K. Müller, K. Müllen, *Acc. Chem. Res.* **2008**, *41*, 1190.
[4] M. Ouchi, T. Terashima, M. Sawamoto, *Chem. Rev.* **2009**, *109*, 4963.
[5] S. Edmondson, V. L. Osborne, W. T. S. Huck, *Chem. Soc. Rev.* **2004**, *33*, 14.
[6] R. R. Bhat, J. Genzer, B. N. Chaney, H. W. Sugg, A. Liebmann-Vinson, *Nanotechnology* **2003**, *14*, 1145.
[7] R. A. Gage, E. P. K. Currie, M. A. Cohen Stuart, *Macromolecules* **2001**, *34*, 5078.
[8] K. C. Grabar, P. C. Smith, M. D. Musick, J. A. Davis, D. G. Walter, M. A. Jackson, A. P. Guthrie, M. J. Natan, *J. Am. Chem. Soc.* **1996**, *118*, 1148.
[9] W. S. Choi, H. Y. Koo, J. Y. Kim, W. T. S. Huck, *Adv. Mater.* **2008**, *20*, 4504.
[10] K. M. Chen, X. Jiang, L. C. Kimerling, P. T. Hammond, *Langmuir* **2000**, *16*, 7825.
[11] H. Zheng, I. Lee, M. F. Rubner, P. T. Hammond, *Adv. Mater.* **2002**, *14*, 569.
[12] A. Ashkin, J. M. Dziedzic, J. E. Bjorkholm, S. Chu, *Opt. Lett.* **1986**, *11*, 288.
[13] H. Lee, J. M. Ferrer, F. Nakamura, M. J. Lang, R. D. Kamm, *Acta Biomater.* **2010**, *6*, 1207.
[14] C.-C. Chiang, M.-T. Wei, Y.-Q. Chen, P.-W. Yen, Y.-C. Huang, J.-Y. Chen, O. Lavastre, H. Guillaume, D. Guillaume, A. Chiou, *Opt. Express* **2011**, *19*, 8847.
[15] M. D. Wang, H. Yin, R. Landick, J. Gelles, S. M. Block, *Biophys. J.* **1997**, *72*, 1335.
[16] U. Bockelmann, Ph. Thomen, B. Essevaz-Roulet, V. Viasnoff, F. Heslot, *Biophys. J.* **2002**, *82*, 1537.

[17] H. D. Ou-Yang, M.-T. Wie, *Annu. Rev. Phys. Chem.* **2010**, *61*, 421.
[18] J. R. Moffitt, Y. R. Chemla, S. B. Smith, C. Bustamante, *Annu. Rev. Biochem.* **2008**, *77*, 205.
[19] K. C. Neuman, S. M. Block, *Rev. Sci. Instrum.* **2004**, *75*, 2787.
[20] G. Cheng, Z. Zhang, S. Chen, J. D. Bryers, S. Jiang, *Biomaterials* **2007**, *28*, 4192.
[21] S. Chen, J. Zheng, L. Li, S. Jiang, *J. Am. Chem. Soc.* **2006**, *127*, 14473.
[22] M. Pluntke, *Organic – Inorganic Interplay in Biomimetic Material Formation*, PhD thesis, Fakultät für Naturwissenschaften der Universität Ulm, **2012**.
[23] A. M. Steinbach, A. Tautzenberger, A. Ignatius, M. Pluntke, O. Marti, D. Volkmer, *J. Mater. Sci. Mater. Med.* **2012**, *23*, 573.
[24] S. A. Letsche, A. M. Steinbach, M. Pluntke, O. Marti, A. Ignatius, D. Volkmer, *Front. Mater. Sci. China* **2009**, *3*, 132.
[25] A. Ziegler, K. Landfester, A. Musyanovych, *Colloid Polym. Sci.* **2009**, *287*, 1261.
[26] S. Tugulu, R. Barbey, M. Harms, M. Fricke, D. Volkmer, A. Rossi, H.-A. Klok, *Macromolecules* **2007**, *40*, 168.
[27] G. Masci, D. Bontempo, N. Tiso, M. Diociaiuti, L. Mannina, D. Capitani, V. Crescenzi, *Macromolecules* **2004**, *37*, 4464.
[28] O. Azzaroni, A. A. Brown, W. T. S. Huck, *Angew. Chem.* **2006**, *118*, 1802; *Angew. Chem. Int. Ed.* **2006**, *45*, 1770.
[29] F. Zhou, Z. Zheng, B. Yu, W. Liu, W. T. S. Huck, *J. Am. Chem. Soc.* **2006**, *128*, 16253.
[30] H.-J. Jacobasch, F. Simon, C. Werner, C. Bellmann, *Tech. Mess.* **1996**, *63*, 439.
[31] H.-J. Jacobasch, F. Simon, C. Werner, C. Bellmann, *Tech. Mess.* **1996**, *63*, 447.
[32] E.-L. Florin, A. Pralle, E. H. K. Stelzer, J. K. H. Hörber, *Appl. Phys. A* **1998**, *66*, S75.
[33] S. F. Tolic-Norrelykke, E. Schäffer, J. Howard, F. S. Pavone, F. Juelicher, H. Flyvbjerg, *Rev. Sci. Instrum.* **2006**, *77*, 103101.